X-RAY PHOTOELECTRON SPECTRA STRUCTURE AND CHEMICAL BONDING IN AmO_2

by

Yury A. TETERIN [1,2*], ***Konstantin I. MASLAKOV*** [2], ***Mikhail V. RYZHKOV*** [3], ***Anton Yu. TETERIN*** [1], ***Kirill E. IVANOV*** [1], ***Stepan N. KALMYKOV*** [2], ***and Vladimir G. PETROV*** [2]

[1] NRC "Kurchatov Institute", Moscow, Russia
[2] Chemistry Department, Lomonosov Moscow State University, Moscow, Russia
[3] Institute of Solid State Chemistry, Ural Department of RAS, Ekaterinburg, Russia

Scientific paper
DOI: 10.2298/NTRP1502083T

Quantitative analysis was done of the X-ray photoelectron spectra structure in the binding energy range of 0 eV to 35 eV for americium dioxide (AmO_2) valence electrons. The binding energies and structure of the core electronic shells (35 eV-1250 eV), as well as the relativistic discrete variation calculation results for the $Am_{63}O_{216}$ and AmO_8 (D_{4h}) cluster reflecting Am close environment in AmO_2 were taken into account. The experimental data show that the many-body effects and the multiplet splitting contribute to the spectral structure much less than the effects of formation of the outer (0- 15 eV binding energy) and the inner (15 eV- 35 eV binding energy) valence molecular orbitals. The filled Am 5f electronic states were shown to form in the AmO_2 valence band. The Am 6p electrons participate in formation of both the inner and the outer valence molecular orbitals (bands). The filled Am $6p_{3/2}$ and the O 2s electronic shells were found to make the largest contributions to the formation of the inner valence molecular orbitals. Contributions of electrons from different molecular orbitals to the chemical bond in the AmO_8 cluster were evaluated. Composition and sequence order of molecular orbitals in the binding energy range 0- 35 eV in AmO_2 were established. The experimental and theoretical data allowed a quantitative scheme of molecular orbitals for AmO_2, which is fundamental for both understanding the chemical bond nature in americium dioxide and the interpretation of other X-ray spectra of AmO_2.

Key words: actinide, X-ray, photoelectron spectrum, valence molecular orbital

INTRODUCTION

Americium is one of the main minor actinides accumulated in the spent nuclear fuel. It has to be extracted, buried or transmutated in nuclear reactors [1-3]. Therefore, much attention is paid to the study of electronic structure of americium and its compounds. The experimental [2-12] and theoretical [13-17] studies of metallic americium and Pu-Am alloys [11] have been conducted. Also the experimental [1, 2, 8, 18-25] and theoretical [21, 26-34] data on the electronic structure of americium oxides have been obtained. The X-ray absorption near-edge spectroscopy (XANES) and extended X-ray absorption fine structure spectroscopy (EXAFS) structures of Am_2O_3 and AmO_2 [20, 23, 28, 31] and americium-containing complex oxides [1,18, 21, 24, 25, 35] have also been studied. The XPS spectra of $Am(NO_3)_3$ n $_2O$ [36], as well as the electron energy loss spectroscopy (EELS) of Am at the Am ($O_{4,5}$) [12] and Am ($N_{4,5}$) [10, 37] absorption edges were measured. The photoelectron spectra are reflected in [2, 8], and the Am 4f X-ray photoelectron spectra (XPS) of Am_2O_3 – in [2, 8, 18]. AmO_2 photoelectron spectrum is given in [22]. XPS spectra of AmO_2 in the wide binding energy (BE) range (0 eV to 900 eV) are given in [19]. It focused on the multiplet splitting related Am 5f structure (0-~15 eV BE). The calculations of AmO_2 electronic structure were conducted mainly for the BE range 0-~15 eV [27, 29-32, 34]. The previous non-relativistic calculations were done for a wider BE range 0- ~25 eV [26]. Unfortunately, these results cannot interpret the valence electrons XPS structure of AmO_2 in the 0-~35 eV BE range.

The XPS study of oxidation states and chemical bond nature in compounds [38] including those of lanthanides [39] and actinides [40] employs peak intensities (I_o), chemical shifts (ΔE_b), BE differences be-

* Corresponding authors; e-mail: Teterin_YA@nrcki.ru

tween core and valence levels (E_i) and spectral structure parameters. The XPS structure can result from formation of the outer (OVMO 0-~15 eV BE) and inner (IVMO ~15 eV-~35 eV BE) valence molecular orbitals [38], spin-orbit splitting (E_{sl}), multiplet splitting (E_{ms}), induced charge (E_{ind}), many-body perturbation (E_{sat}), dynamic effect (gigantic Coster-Kronig transitions), Auger process, *etc*. [39, 40]. These structure parameters provide information on: degree of delocalization and participation of electrons in chemical binding; electronic configuration and oxidation states of ions; density of uncoupled electrons on paramagnetic ions; degree of participation of filled electronic shells of metals and ligands in the OVMO and IVMO formation, structure and nature of the MO; local environment structure, *etc*. [38-43].

The valence XPS (0-~35 eV BE) structure with the photoionization cross-sections in mind reflects the total valence density of occupied states. Beside the MO structure this BE range can exhibit an extra structure due to the multiplet splitting, many-body perturbation etc. This extra XPS structure can be interpreted taking into account the data on the core electron (0-1250 eV BE) XPS structure. It allows one to evaluate contributions of different mechanisms of the extra structure formation to the valence XPS [41-43].

The XPS peaks of actinide oxides in the BE range 0-~35 eV were found to be several eV wide, which sometimes is wider than the corresponding core electron peaks [41-43]. For example, the O 1s peak (E_b = 529.0 eV) full width at half maximum (FWHM) (Γ, eV) for AmO_2 is Γ = 1.3 eV, while the corresponding O 2s (E_b~20.9 eV) peak is ~4.0 eV wide and structured. It contradicts the Heisenberg uncertainty ratio $E \tau \quad h/2$, where E is the natural width of a level from which an electron was extracted, τ is the hole lifetime and h is Planck constant. Since the hole lifetime (τ) grows as the absolute atomic level energy decreases, the lower BE XPS atomic peaks are expected to be narrower. For AmO_2 and other actinide oxides [41-44] it is *vice versa*. This fact allowed a suggestion [44] that beside electrons from incompletely filled shells of the neighboring ions (0-~15 eV BE), electrons from the filled shells (15 eV-~35 eV BE) can effectively (experimentally observed) participate in the chemical bond formation. This fact stimulated experimental and theoretical studies of the low BE (~15 eV to ~35 eV) XPS structure in oxides of actinides [40], lanthanides [39], and other compounds [38]. One of the reasons for such an XPS structure formation was established to be the IVMO and the OVMO formation with significant participation of the An 6p and the O 2s filled atomic shells [40, 44] Practically, the low energy spectra reflect the valence band (0-~35 eV) structure. They are observed as bands several eV wide.

The XPS of the low BE (0-~35 eV) electrons from AmO_2 [19] was measured and the theoretical calculations of the electronic structure of AmO_2 in the energy range 0-~25 eV in the non-relativistic cluster approximation of the X_α discrete variation method (X_α DVM) [26] were done before. It allowed only a qualitative interpretation of the low BE XPS from AmO_2. Unfortunately, the calculation results for AmO_2 [27-33] for the BE range 0-~15 eV did not take into account the overlapping of the inner valence Am 6p and the O 2s atomic orbitals and, therefore, did not allow a correct valence (~15 eV-~35 eV) XPS structure interpretation.

The XPS studies of americium [2-9] and oxides AmO_x [2, 8, 18, 19, 22] focused attention on the outer valence (0-~15 eV BE) and the core Am 4f electron spectra. The Am 4f XPS structure is significantly different for metallic Am and its oxides. However, the XPS structure of the inner valence electrons of AmO_2 in the BE range ~15 eV-~35 eV was not studied. The authors of [19, 36, 40] did not study the inner Am 4p, 4d, 5s, 5p, 5d, and 6s electronic structures. The absence of the experimental Am 4p, 5s, 5p and 6s XPS of AmO_2 did not allow an interpretation and the theoretical modeling of the XPS structure of this BE range.

The quantitative interpretation of the valence XPS structure in the BE range 0-~35 eV taking into account the photoelectron, conversion, emission and other X-ray spectral data and relativistic calculation results was done for ThO_2 [45], UO_2 [46], NpO_2 [43], PuO_2 [41], ThF_4 [47], UF_4 [48], UO_2F_2 [49], and γ-UO_3 [50]. The present work analyzed the XPS from AmO_2 in the BE range 0-1250 eV and quantitatively interpreted the XPS structure in the BE range 0-~35 eV. The binding energies and core electron spectral structure parameters as well as the relativistic self-consisting field discrete variation (SCF RDV) calculation results for the AmO_8 (D_{4h}) cluster reflecting Am close environment in AmO_2 were taken into consideration.

EXPERIMENTAL

Samples

The AmO_2 sample for the XPS studies was prepared as a dense thin layer on a platinum substrate (3-4 mm diameter AmO_2 sample on 14 mm diameter foil).

AmO_2 synthesis

The nitrate solution containing the necessary amount of Am (~$10^{18\text{-}19}$ atoms) was gradually placed on the platinum substrate and dried under a 500 W incandescent lamp. Then the sample was annealed in a muffle furnace for 4 hours at 800 °C. AmO_2 formation on the substrate surface was controlled by XPS on the basis of the O 1s, Am 4f and valence electrons parameters. It allowed a sample of the stoichiometric compo-

sition close to AmO_2 with excess oxygen on the surface. The surface of the prepared sample was etched with argon ions at 2 keV and 50 A for 10 and 30 s. Unfortunately, the Ar treatment leads to formation of oxide with spectral parameters similar to Am_2O_3 on the surface (tab. 1).

X-ray photoelectron measurements

XPS spectra of AmO_2 were measured with an electrostatic spectrometer Kratos Axis Ultra DLD (Kratos Analytical Ltd., Great Britain) using $AlK_{\alpha 1,2}$ ($h\nu$ = 1486.6 eV) radiation under 5 10^{-7} Pa at room temperature. The informative surface was 300 700 m^2. The device resolution measured as FWHM of the Au $4f_{7/2}$ peak was 0.7 eV. The binding energies E_b(eV) were measured relatively to the BE of the C 1s electrons from hydrocarbons absorbed on the sample surface that was accepted to be equal to 285.0 eV. The C 1s XPS on the studied sample surface was observed as a low-intensity peak at E_b(C 1s) = 285.0 eV. The error in the determination of the binding energy and the peak widths did not exceed 0.1 eV, that of the relative peak intensity – 10 %. The FWHMs are giver relatively to that of the C 1s XPS peak from hydrocarbon on the sample surface being 1.3 eV [40]. The background due to the inelastically scattered electrons was subtracted by the Shirley method [51].

The valence and the core electron XPS structure for the studied sample in the BE range 0-1250 eV is typical for AmO_2. It confirms unambiguously the presence of AmO_2 on the substrate surface [40]. A low-intensity Pt 4f doublet at E_b(Pt $4f_{7/2}$) = 71.0 eV and E_{sl} = = 3.3 eV was observed. It evaluated the Pt $5d^96s^1$ contribution to the AmO_2 valence band (0-15 eV BE) XPS intensity not more than 1 percent and it was taken into account. The core and valence XPS from metallic Pt were taken, the binding energy E_b(Pt $4f_{7/2}$)=70.8 eV, the spin-orbit splitting E_{sl}(Pt $4f_{7/2}$) = 3.3 eV and the FWHM Γ(Pt$4f_{7/2}$) = 0.9 eV were measured. The valence band (VB) was observed in the BE range 0 eV-10 eV with peaks at 0.2, 1.4, and 4.0 eV, general FWHM Γ(VB) = 5.8 eV and the valence band to the Pt $4f_{7/2}$ peak intensity ratio I(VB)/I(Pt$4f_{7/2}$) = 0.16.

Quantitative elemental analysis of layers several nanometer-deep of the studied samples was done based on the fact that the spectral intensity is proportional to the number of certain atoms in the studied sample. The following ratio was used: n_i/n_j = = $(S_i/S_j)(k_j/k_i)$, where n_i/n_j is the relative concentration of the studied atoms, S_i/S_j is the relative core-shell spectral intensity, k_j/k_i is the relative experimental sensitivity coefficient. The following coefficients relative to the C 1s were used: 1.00 (C 1s); 2.80 (O 1s); 43.36 (Am$4f_{7/2}$; see, *e. g*. [52]). The best stoichiometric composition of americium dioxide was $AmO_{2.09}$ and $AmO_{1.56}$ (Am_2O_3), taking into account the main core O 1s and the Am $4f_{7/2}$ peaks with shake-up satellites.

CALCULATIONS

Electronic structure calculations of AmO_2 were made for the two types of finite fragments of crystal lattice: a 279-atom cluster $Am_{63}O_{216}$ and a AmO_8 cluster.

Table 1. Electron BE E_b [eV] and photoionization cross-sections σ[a] at 1487 eV

Am nlj O nlj	AmO_2	AmO_2[b]	Am_2O_3	$Am(NO_3)_3$ nH_2O[(c)]	Am[(d)]	Am_{Theor}[(e)]	σ
Am $5f_{7/2}$						2.99	35.1
Am $5f_{5/2}$	2.2 (1.6)		1.7(1.6)	4.5	2.8	5.58	28.3
Am $6p_{3/2}$	17.3 (3.0)	18.1	17.1(3.1)	19.8	18.4	23.29	5.36
Am $6p_{1/2}$	30.8(1.9)	31.1	30.5(2.5)	32.9		35.84	1.77
Am 6s	49.8(7.0)		47.5(7.6)			57.98	2.39
Am $5d_{5/2}$	108.2(2.8)	108.4	107.6(2.8)	109.9		113.15	53.4
Am $5d_{3/2}$						129.34	36.3
Am $5p_{3/2}$	217.8		217.2	219.6		234.13	33.7
	222.8		224.2				
Am $5p_{1/2}$	~289		~289			303.68	9.24
Am 5s						376.15	10.6
Am $4f_{7/2}$	448.2(2.6)	448.2	447.6(2.5)	449.9	446.4	450.84	451
Am $4f_{5/2}$	462.2(2.8)	462.5	461.8(3.2)	464.5		465.40	353
Am $4d_{5/2}$	832.5(5.8)	832.0	831.7(5.9)	834.0		839.15	247
Am $4d_{3/2}$	883.5(5.8)	883.1	882.5(5.7)	884.9		890.06	160
Am $4p_{3/2}$	1164.2(6.9)		1163.8(8)	1165.8		1173.26	111
O 2p	~4.0						0.27
O 2s	~21	23.1		26.5			1.91
O 1s	529.0(1.3)	529.0	528.9(1.3)	533.1			40
N 1s				407.7			24.5

[(a)] Photo-ionization cross-sections σ (kilobarn per atom, *i. e*., 10-25 m^2 per atom) [68, 70]; [(b)] values for AmO_2 from [19];
[(c)] values for $Am(NO_3)_3$ nH_2O from [36]; [(d)] values for metallic Am [4, 7, 8]; [(e)] calculation data [59]

The latter object reflecting Am close environment in AmO_2 is a body-centered cube with Am in the center and eight oxygens in the corners. The Am-O interatomic distance $R_{Am\text{-}O}$ = 0.23287 nm [20, 23, 53]. For the modeling of boundary conditions for the $Am_{63}O_{216}$ we used the "extended cluster" scheme [54]. In this model, the crystal fragment under study consists of two parts: the internal main part (or the core of the cluster) and the outer part (or the shell). The latter part usually includes the atoms of 1-5 co-ordination spheres surrounding the core. During the self-consistent procedure, the electron densities and the potential of the ions in the shell are replaced by the corresponding values obtained for the crystallographically equivalent centers of the cluster core. To introduce the long-range component of the surrounding crystal potential, the extended cluster is embedded in a pseudopotential of the outer crystal lattice, including several thousand centers with Coulomb and exchange-correlation potentials obtained for the corresponding equivalent atoms in the internal part of the cluster.

In the case of $Am_{63}O_{216}$, the core of the cluster included the Am atom in the center (Am1), with eight nearest oxygen neighbors (O1), and 12 americium sites of the next actinide co-ordination sphere with their 48 nearest oxygen atoms. The other atoms of the cluster formed the shell and during self-consistency calculations, their electronic densities and potentials were kept equivalent to those of Am1 and O1. In the case of the small fragment AmO_8, the re-normalization procedure for the oxygen atom's valence orbital populations during the self-consistency calculations was used. The latter model of a small cluster boundary condition also allows one to include into the iterative scheme the stoichiometry of the compound and the possibility of charge redistribution between outer atoms in the cluster and the surrounding crystal.

In the present paper, the electronic structure is calculated in the density functional theory (DFT) approximation using the original code of the fully relativistic discrete variation (RDV) cluster method [55] with exchange-correlation potential [56]. The RDV method is based on the solution of the Dirac-Slater equation for 4-component wave functions transforming according to the irreducible representations of the double point group (D_{4h}; in the present calculations). For the calculation of symmetry coefficients, we used the original code, which realizes the projection operators technique and includes the matrices of the irreducible representations of double point groups [57] and the transformation matrices presented in [58]. The extended basis of the 4-component numerical atomic orbitals (AO) obtained as the solution of the Dirac-Slater equation for the isolated neutral atoms also included the Am $7p_{1/2}$ and the Am $7p_{3/2}$ functions in addition to the occupied AO. The use of such "most natural basis orbitals" and the absence of any muffin-tin (M-T) approximation to potential and electronic density allow one to describe the formation of inter-atomic bonds. In such an approach, this description is more illustrative than that obtained in the band structure approach. Numerical Diophantine integration in matrix elements calculations was carried out for 700000 ($Am_{63}O_{216}$), and 22000 (AmO_8) sample points distributed in the cluster space. It provided the convergence of MO energies better than 0.1 eV.

RESULTS AND DISCUSSION

As it was mentioned above, the valence (0-~35 eV BE) XPS structure of AmO_2 can be attributed not only to the OVMO and IVMO formation, but to other mechanisms as well. In order to evaluate the contribution of other mechanisms in the valence XPS, the core electron XPS structure of AmO_2 was analyzed.

Core-electron XPS structure of AmO_2

The O 1s XPS of AmO_2 was observed as a single peak at E_b(O 1s) = 529.0 eV and FWHM Γ(O 1s) = = 1.3 eV (fig. 1) with a shoulder at E_b(O 1s) = 530.7 eV at the higher BE side from the basic peak attributed to hydroxyl groups and another shoulder at E_b(O 1s) = = 532.2 eV. The peak intensity ratio yielded 50 % of AmO_2, 34 % of OH^-, and 16 % of H_2O. The O 2p and the O 2s intensities from the OH^- and H_2O impurities increase the errors in the valence XPS decomposition.

The Am 4f XPS from AmO_2 at the highest probability shows the many-body perturbation-related structure attributable to an extra electronic transition within the filled and the vacant valence levels during the Am 4f photoemission. It appears as shake-up satellites, whose parameters reflect the MO structure. As a result, the Am 4f XPS consists of the spin-orbit split doublet with E_{sl}(Am 4f) = 14.1 eV, and the shake-up satellites at the higher BE side with E_{sat} = 6.9 eV (fig. 2). The satellite intensity ($I_{sat} = I_s/I_o$) calculated as the

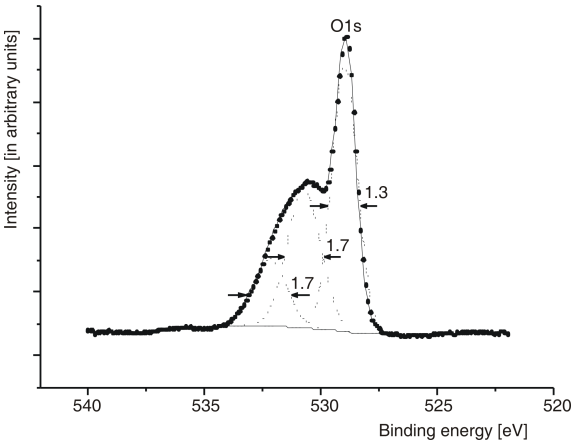

Figure 1. O 1s XPS from AmO_2

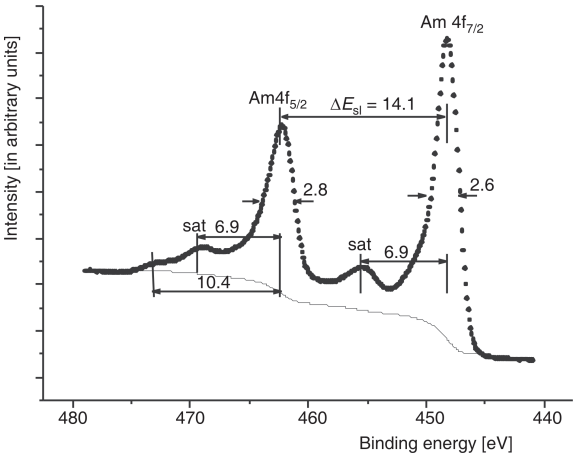

Figure 2. Am 4f XPS from AmO_2

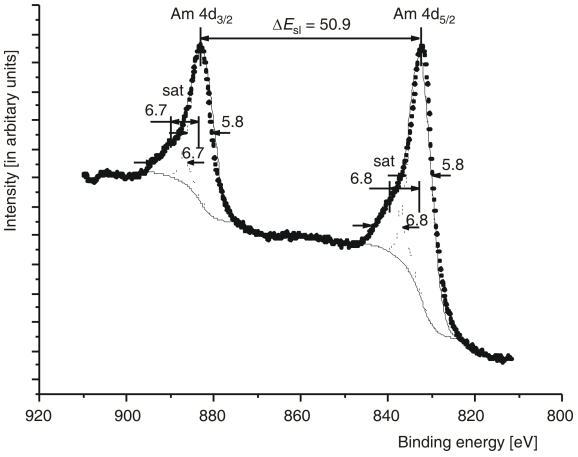

Figure 3. Am $4d_{5/2}$ XPS from AmO_2

ratio of the XPS satellite area (I_s) to the basic peak area (I_o) was 20 %. The Am 4f XPS structure is typical for the Am(IV) [19] oxidation state and differs from that for Am(III) in Am_2O_3 [2, 18] and $Am(NO_3)_3 \times nH_2O$ [36], which exhibits the satellites at E_{sat} 2.5 eV. In the present work, such satellites in the Am 4f XPS of Am_2O_3 were observed at E_{sat} 2.8 eV. Such typical satellites with E_{sat} = 6.9 eV are observed in all the An 4f XPS of dioxides AnO_2 (An = Th, U, Np, Pu) [19, 40, 41, 43]. For example, for PuO_2 [41] these typical shake up satellites appear in the spectra of various shells in the BE range 0-1250 eV, and their intensities decrease as the BE decrease. Indeed, the Am $4d_{5/2}$ XPS with $E_b(Am\ 4d_{5/2}) = 832.5$ eV and $\Gamma(Am\ 4d_{5/2}) =$ = 5.8 eV at $E_{sat}(Am4d_{5/2}) = 6.9$ eV from the higher BE side also shows the shake-up satellite with $I_{sat} =$ = 25 % (fig. 3). The extrapolation of the shake-up satellite intensities predicts yields the valence shake up satellite intensity to be ~15 %.

The multiplet splitting caused by the presence of the uncoupled Ln 4f electrons in lanthanide compounds results, *e. g.*, in the Ln 4d XPS structure [39]. Therefore,

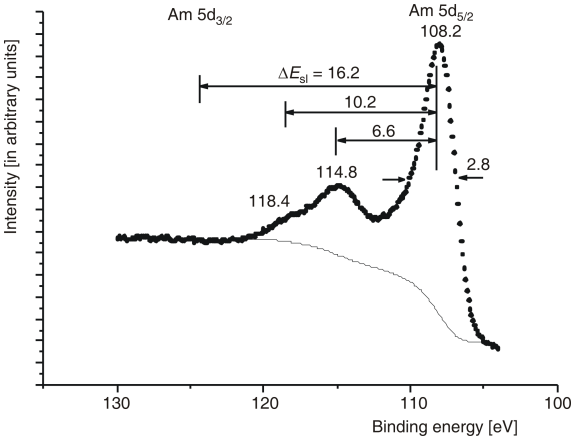

Figure 4. Am $5d_{5/2}$ XPS from AmO_2

the multiplet splitting was expected to appear with the higher probability in the An 5d XPS [40, 41, 43]. Indeed, the Am 5d spectrum instead of a spin-orbit split doublet ($E_{sl}(Am\ 5d)_{theor.} = 16.19$ eV [59]) exhibits a complicated structure with the Am $5d_{5/2}$ maximum at 108.2 eV (fig. 4, tab. 1). This structure can be explained by the multiplet splitting superimposed with the shake-up satellites. Therefore, it is difficult to separate the satellite-related structure and to determine the satellite intensities. The multiplet splitting is very likely to appear in the Ln 4s XPS from lanthanide oxides [39]. In the Ln 5s XPS the probability is about twice as low. Therefore, the Am 5s and the Am 6s XPS are expected to exhibit the multiplet splitting.

To evaluate the multiplet splitting in the Am 5s and the Am 6s XPS one can use the simplified expression for an ion with uncoupled electrons [43, 60]. An ion with an incompletely filled valence shell electronic configuration nl^v, for example, the Am $5f^5$ for Am(IV), has two final states after the electron photoemission from the core *n's* shell. They are formed from the configurations *n's* and nl^v. The energy difference E_{ms} between these two states in this approximation is [43, 60]

$$\Delta E_{ms} \quad \frac{2S}{2l}\frac{1}{1} G^1(n,s,nl) \qquad (1)$$

where *S* is the initial spin attributable to the coupling of the *nl* electrons (*n* and *l* are the principal and orbital quantum numbers), $G^l(n's, nl^v)$ is the corresponding atomic exchange Slater integral, *e. g.*, for the Am(IV) ion with 5 uncoupled electrons [36]. From (1) it follows that E_{ms} is proportional to the multiplicity $(2S + 1)$ or to the number of the uncoupled electrons in the ion. The intensity ratio of the doublet components I_1/I_2 has to be equal to the ratio of the multiplicities of the final states [60]

$$\frac{I_1}{I_2} \quad \frac{S}{S}\frac{1}{} \qquad (2)$$

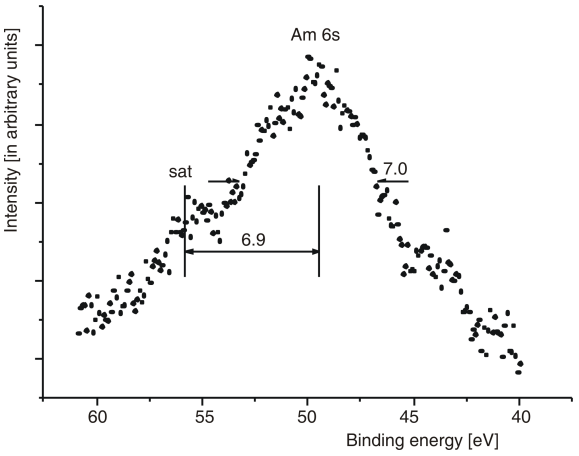

Figure 5. Am 6s XPS from AmO_2

In this approximation, for the Am(IV) ion with the electronic configuration $Am5f^5$ and the Slater integral $G^3(5s,5f) = 7.81$ eV (for Np) [43] the Am 5s multiplet splitting is $E_{ms}(Am\ 5s) = 6.69$ eV and the Am 5s doublet intensity ratio is 7:5, while for $G^3(6s, 5f) = 5.26$ eV (for Np) [43], the splitting is $E_{ms}(Am\ 6s) = 4.51$ eV and the intensity ratio in the Am 6s doublet is also 7:5.

The Am 6s XPS structure can be considered to contain a $E_{ms}(Am\ 6s) = 4.5$ eV split doublet with the intensity ratio of 7:5 (fig. 5). In reality, this XPS structure is more complicated. It can be explained by the many-body perturbation and the dynamic effect related structure. This process was studied earlier for the Th 5p XPS structure from metallic Th [61] and Th and U compounds [62, 63]. Reference [62] presents the interaction integrals of different configurations for thorium. These data show that the dynamic effect has to manifest with the highest probability in the An 5p and An 5s XPS, it is also highly probable in the An 6s XPS.

The dynamic effect is related to the gigantic Coster-Kronig transitions, *e. g.* the one observed in the Am 5p XPS. It appears as the two peaks in the Am $5p_{3/2}$ doublet component at 217.8, and at 222.8, eV and the structure in the Am $5p_{1/2}$ BE range at ~289 eV (tab. 1). The similar splitting was observed in the Pu $5p_{3/2}$ XPS from PuO_2 [19, 41]. With the data on the Ba 4p [64] and the Ln 4p [39, 65, 66] XPS in mind, one can attribute the Am 5p structure to the dynamic effect. It results in the Am ion complex final state consisting of the ground one-hole state $Am5p^55d^{10}5f^n$ and the excited two-hole $Am\ 5p^65d^85f^{n+1}$ state. Indeed, this suggestion is based on the Am 5p and the Am 5d binding energy ratio $E_b(Am\ 5p_{3/2})$ 220 eV and $E_b(Am\ 5d_{5/2})$ = 108.2 eV, which satisfies the condition: $E_b(Am\ 5p_{3/2})$ 2 $E_b(Am\ 5d_{5/2})$ (tab. 1). As a result, the probability of an extra excited two-hole final $Am\ 5p^65d^85f^{n+1}$ state grows.

The Am 5s XPS is expected around $E_b(Am\ 5s)$ ~373.3 eV, as it follows from the internal electron conversion data [67] and agrees qualitatively with the calculation results (376.15 eV) (tab. 1, [59]). However, the Am 5s XPS was not interpreted because of its complicated and blurred structure, which can be attributed to both the multiplet splitting and the dynamic effect [40].

The dynamic effect leads to the interaction of the configurations of the final states $Am\ 5s^15p^65d^{10}5f^n$ and $Am\ 5s^25p^55d^95f^{n+1}$. Indeed, for the Am 5s, Am 5p and Am 5d binding energies (tab. 1) the condition $E_b(Am\ 5s)$ $E_b(Am\ 5p) + E_b(Np5d_{3/2})$ is satisfied, which does not contradict the possibility of the suggested configurations. The binding energies $E_b(Am\ 4p_{3/2}) = 1164.2$ eV, $E_b(Am\ 4d_{3/2}) = 883.5$ eV and $E_b(Am\ 5s) \sim 373$ eV satisfy the condition $E_b(Am\ 4p_{3/2}) \sim E_b(Am\ 4p_{3/2}) + E_b(Am\ 5s)$. Therefore, the Am $4p_{3/2}$ XPS structure of AmO_2, to a certain extent, can be attributed to the dynamic effect with the interaction of the configuration of the final states $Am\ 4p^54d^{10}5s^25f^n$ and $Am\ 5p^64d^95s^14f^{n+1}$. Shake-up satellites can be superimposed with this structure.

The Am 6s XPS exhibits a widened [$\Gamma(Am\ 6s) = 7.0$ eV] structured line at 49.8 eV (fig. 5). One of the reasons for such structure, as it was already noted, is the multiplet splitting. Another reason for this structure can be the dynamic effect resulting in the interaction of the configurations of the Am(IV) ion final states like $Am\ 6s^16p^66d^05f^5$ and $Am\ 6s^26p^46d^15f^5$. Indeed, for the BE $E_b(Am\ 6s) = 49.8$ eV, $E_b(Am\ 6p_{3/2}) = 17.3$ eV, and $E_b(Am\ 6p_{1/2}) = 30.8$ eV (tab. 1), the condition $E_b(Am\ 6s)$ 2 $E_b(Am\ 6p)$ is met. These XPS can also exhibit extra structures related to the multiplet splitting and shake-up satellites. Therefore, the considered XPS structure cannot allow a conclusion on the participation of the Am 6s electrons in the MO formation.

The measured Am 4f BEs and structure parameters agree with the corresponding data obtained earlier for AmO_2 [19]. Since the XPS structure in the An 6p BE range ongoing from ThO_2 to NpO_2, PuO_2, and AmO_2 does not differ significantly by the shape [19, 40, 41, 43], while the number of the quasi-atomic An 5f electrons grows from 0 to 5, one can suggest that the multiplet splitting does not play a primary role in the valence XPS structure formation in the BE range ~15 eV-~35 eV. The dynamic effect-related structure is also low probability in this BE range, because of the atomic states but, the quasi-atomic Am 5f ones at 2.2 eV BE (tab. 1) are absent in the valence band. As a result, a suggestion that the valence XPS structure can be largely attributed to the MO formation, except for the peak at 8.8 eV, can be drawn (fig. 6). The peak at 8.8 eV is 6.6 eV away from the peak of the localized Am 5f electrons $E_b(Am\ 5f) = 2.2$ eV and therefore, can be attributed to the many-body perturbation (shake-up satellites in the XPS of the quasi-atomic Am 5f electrons). However, as it was shown in [41], intensity of such a satellite cannot exceed several percent of the basic peak. Another reason for such a peak can be the

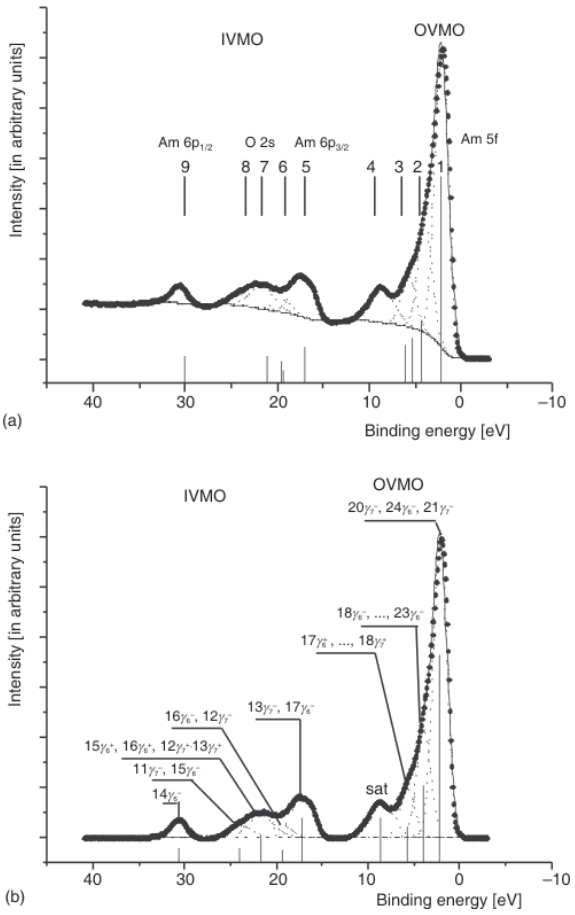

Figure 6. Valence band XPS from AmO_2: (a) – spectrum with the secondarily scattered electrons background. The dashed lines show the division of the spectrum into separate components, vertical bars show the calculated (RDV) spectrum; (b) – spectrum with subtracted background. The dashed lines show the division of the spectrum into separate components, vertical bars show the correct expected spectrum

surface oxygen [68]. The obtained data also allow a conclusion that the studied sample by its stoichiometry is close to AmO_2. For the interpretation of the MO-related valence band XPS structure, the results of electronic structure calculations of the finite clusters AmO_8 (D_{4h}) as well as the $Am_{63}O_{216}$ cluster (fig. 7) reflecting Am close environment in AmO_2 ,were used.

Electronic structure of the AmO_8 and $Am_{63}O_{216}$ clusters

Americium atom ground-state configuration can be presented as $[Rn]6s^26p^65f^76d^07s^27p^0$, where [Rn] is radon electronic configuration and the other electronic shells are valence and can participate in the interatomic binding with oxygen atoms ($O\ 2s^22p^4$). The total densities of occupied states obtained for the central Am1 and O1 atoms in the two clusters are shown in fig. 7. A comparison of the DOS in fig. 7 shows that the

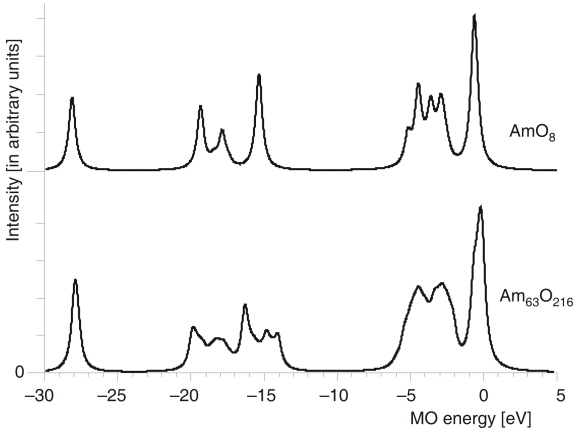

Figure 7. Total DOS for the central part of $Am_{63}O_{216}$ and AmO_8 clusters obtained in RDV calculations

widths of energy bands noticeably increase on going from small AmO_8 fragment to a large $Am_{63}O_{216}$ cluster (we have broadened each MO level with a Lorentzian function of constant small width 0.01 eV) for all MO. The obtained data show that the gravity centers of the main bands in both fragments are close to each other. Moreover, the analysis of the covalent mixing of the Am $6p_{1/2}$, $6p_{3/2}$ with the O 2s orbitals and the Am $5f_{5/2}$, $5f_{7/2}$, $6d_{3/2}$, $6d_{5/2}$, 7s, $7p_{1/2}$, and $7p_{3/2}$ with the O 2p AO shows that the primary features of hybridization between metal and oxygen states are also similar in both clusters. Since the 279-atomic fragment in the energy region under investigation (0-~ 35 eV) contains 2357 orbitals, for illustration of general structure of the primary molecular states, we use the results of the RDV calculations for the small AmO_8 cluster, which models only the nearest environment of Am in AmO_2. The characteristics of all vacant and occupied MO in the energy region from +10 to –50 eV obtained for this cluster are given in tab. 2.

Since the RDV method is based on the MO expression as linear combination of AO (LCAO), this approach allows one to use both atomic and molecular terms for the chemical bond description.

Indeed, the chemical bond formation and the Am and O atomic shells overlapping, result in the OVMO and IVMO formation. These OVMO and IVMO beside the Am 6s,6p,5f,6d,7s, and O 2s,2p AO include also the filled Am 7p states, which are absent in atomic americium. Unlike the non-relativistic calculation for AmO_2 [26], whose results showed a significant participation of the Am 6s AO in the MO formation, the relativistic calculation yielded the results showing that the Am 6s AO practically do not participate in the MO formation (tab. 2). The Am 7s and Am 7p AO take a significant part in the MO formation. While the Am 5f AO participate mainly in the OVMO formation, the Am 6p,6d AO participate in both the OVMO and the IVMO formation. The largest Am $6p_{3/2}$-O 2s AO mixing of the neighboring americium and oxygen was ob-

Table 2. MO compositions and energies E_0 [(a)] [eV] for the AmO_8 cluster (RDV) and photoionization cross-sections σ_i [(b)]

MO		$-E_0$ [eV]	MO composition												
			Am											O	
			6s σ_i [(a)] 1.18	$6p_{1/2}$ 0.88	$6p_{3/2}$ 1.33	$6d_{3/2}$ 0.64	$6d_{5/2}$ 0.57	7s 0.11	$5f_{5/2}$ 4.72	$5f_{7/2}$ 4.38	$7p_{1/2}$ 0.05	$7p_{3/2}$ 0.06	2s 0.96	$2p_{1/2}$ 0.07	$2p_{3/2}$ 0.07
OVMO	$22\gamma_7^+$	–9.57					0.85						0.05	0.08	0.02
	$25\gamma_6^+$	–9.36				0.45	0.39						0.05	0.01	0.10
	$21\gamma_7^+$	–9.35				0.45	0.39						0.05	0.02	0.09
	$24\gamma_6^+$	–7.10						0.89					0.06	0.02	0.03
	$28\gamma_6^-$	–6.11								0.01	0.91		0.04	0.02	0.02
	$20\gamma_7^+$	–6.08				0.39	0.47							0.04	0.10
	$23\gamma_6^+$	–6.07				0.39	0.47							0.04	0.10
	$27\gamma_6^-$	–4.63			0.01							0.92	0.03		0.04
	$24\gamma_7^-$	–4.56										0.92	0.02		0.06
	$23\gamma_7^-$	–1.72							0.06	0.73			0.01	0.10	0.10
	$26\gamma_6^-$	–1.08								0.89				0.10	0.01
	$22\gamma_7^-$	–1.05								0.89				0.02	0.09
	$25\gamma_6^-$	–1.04							0.01	0.89				0.02	0.08
	$21\gamma_7^-$ [(c)]	0.00							0.72	0.13				0.02	0.13
	$24\gamma_6^-$	0.13							0.79	0.02				0.01	0.18
	$20\gamma_7^-$	0.14			0.01				0.79	0.01			0.01	0.01	0.17
	$23\gamma_6^-$	1.95												0.32	0.68
	$19\gamma_7^-$	1.95												0.32	0.68
	$22\gamma_6^+$	2.16												0.16	0.84
	$19\gamma_7^+$	2.17												0.14	0.86
	$21\gamma_6^+$	2.18												0.66	0.34
	$22\gamma_6^-$	2.37			0.04				0.13	0.03				0.17	0.63
	$18\gamma_7^-$	2.37			0.04				0.13	0.03				0.31	0.49
	$18\gamma_7^+$	2.43												0.04	0.96
	$17\gamma_7^+$	2.46												0.50	0.50
	$20\gamma_6^+$	2.47												0.50	0.50
	$21\gamma_6^-$	2.75								0.10	0.01			0.79	0.09
	$17\gamma_7^-$	3.06							0.14	0.11				0.28	0.47
	$16\gamma_7^-$	3.12			0.01				0.03	0.01		0.05		0.19	0.71
	$20\gamma_6^-$	3.12							0.03	0.01		0.05		0.09	0.82
	$19\gamma_6^-$	3.43									0.04		0.01	0.30	0.65
	$16\gamma_7^+$	3.86				0.01	0.09						0.01	0.55	0.34
	$19\gamma_6^+$	3.90				0.06	0.04						0.01	0.02	0.88
	$15\gamma_7^+$	3.89				0.05	0.04						0.01	0.35	0.55
	$18\gamma_6^+$	3.97						0.04					0.01	0.33	0.62
	$15\gamma_7^-$	3.99							0.05	0.05				0.17	0.73
	$18\gamma_6^-$	3.99							0.04	0.05				0.16	0.75
	$14\gamma_7^-$	4.01							0.07	0.03				0.55	0.35
	$14\gamma_7^+$	4.64				0.06	0.08							0.28	0.58
	$17\gamma_6^+$	4.65				0.06	0.08							0.28	0.58
IVMO	$17\gamma_6^-$	14.83			0.58							0.02	0.35	0.01	0.03
	$13\gamma_7^-$	14.83			0.59							0.02	0.35	0.01	0.03
	$12\gamma_7^-$	16.93							0.01	0.01			0.98		
	$16\gamma_6^-$	17.34		0.02							0.04		0.94		
	$13\gamma_7^+$	17.35					0.06						0.94		
	$12\gamma_7^+$	17.35				0.04	0.02						0.94		
	$16\gamma_6^+$	17.35				0.04	0.02						0.94		
	$15\gamma_6^+$	17.93						0.07					0.93		
	$15\gamma_6^-$	18.82			0.36								0.62		0.01
	$11\gamma_7^-$	18.82			0.36								0.61	0.01	
	$14\gamma_6^-$	27.60		0.98									0.02		
	$14\gamma_6^+$	47.63	1.00												

[(a)] Energies shifted upward by 13.67 eV; [(b)] photoionization cross-section σ_i (kilobarn per electron) [68, 70]; [(c)] highest filled MO (1 electron), occupation number for all the orbitals 2

served for the $17\gamma_6^-$,$13\gamma_7^-$ (5) and $15\gamma_6^-$,$11\gamma_7^-$ (8) IVMO (tab. 2). The Am $6p_{1/2}$ and the O 2s AO mixing of the neighboring americium and oxygen for the $16\gamma_6^-$ (6) and $14\gamma_6^-$ (9) IVMO is significantly less than for the corresponding orbitals in ThO_2 [69] and UO_2 [70]. This can be explained by the increase in the spin-orbit splitting energy E_{sl}(An 6p) and the An $6p_{1/2}$ BE relative to the O 2s BE as the atomic number Z grows in the actinide row. These results allow one to understand the valence electrons XPS spectral structure of AmO_2.

Valence XPS structure of AmO_2

The XPS from AmO_2 in the BE range 0-~35 eV can be conditionally subdivided into two ranges, fig. 6(a). The first range 0-~15 eV exhibits the OVMO-related structure. These OVMO are formed mostly from the Am 5f, 6d, 7s, 7p, and the O 2p AO of the neighboring atoms. The second range ~15 eV-~35 eV exhibits the IVMO-related structure. These IVMO appear mostly due to the strong interaction of the completely filled Am 6p and O 2s AO. The OVMO XPS structure has its typical features and can be subdivided into four components (1- 4). The results of the OVMO XPS division into the three components at 2.2, 4.0, and 5.8 eV (fig. 6, tab. 3) agree with the UV spectroscopy data for americium dioxide [22]. The UV photoelectron spectrum of AmO_2 also exhibits the three peaks around 2, 4, and 6 eV. However, the UV and the XPS intensities of these peaks differ significantly since the O 2p and the Am 5f photoionization cross-sections are comparable at He II (40.81 eV) excitation, while at the AlK (1486.6 eV) excitation the Am 5f photoionization cross-section is more than 50 times higher than the O 2p one (tab. 2, [71]). The growth of the peak at 2 eV in the UV photoelectron spectrum of Am_2O_3 as the excitation energy increases on going from He I (21.22 eV) to He II (40.81 eV) confirms that this peak belongs to the Am 5f electrons [8].

The IVMO range exhibits explicit peaks and can be subdivided into five components 5-9; fig. 6(a). Despite the formalism of such a division, it allows qualitative and quantitative comparison of the XPS parameters with the relativistic calculation results for the AmO_8 cluster.

Results of these calculations are given in tab. 2. Since photoemission results are given for an excited state of an atom with a hole on a certain shell, the calculations must be done for transition states for a stricter comparison of the theoretical and experimental BE [72]. However, the valence electrons BE calculated for transition states are known [38-40] to differ from the corresponding values for the ground state by a constant shift toward the higher energies. Therefore, the present paper gives the calculated BE (tab. 2) shifted by 2.17 eV (tab. 3). Taking into account the MO compositions (tab. 2) and the photoionization cross-sections [71, 73], the theoretical intensities of several XPS ranges were determined (tab. 3). Comparing the experimental XPS to the theoretical data, one should keep in mind that the XPS from americium dioxide reflects the band structure and consists of bands widened due to the solid-state effects. Despite this approximation, a satisfactory qualitative agreement between the theoretical and the experimental data was obtained, fig. 6(a). The corresponding theoretical and experimental FWHM and the relative intensities of the inner and outer valence bands are comparable tab. 3, fig. 6(a). A satisfactory agreement between the experimental and calculated BE of some MO was also reached (tab. 3). The worst discrepancy was observed for the middle IVMO XPS ($12\gamma_7^+$-$15\gamma_6^-$). As mentioned, the NR X -DVM [26] results allowed only qualitative interpretation of the low BE XPS of AmO_2. The present relativistic calculations practically allow a quantitative identification of the valence XPS structure of AmO_2 in the whole BE range of 0 eV to ~35 eV, tab. 3, fig. 6(b). The expected correct spectrum obtained on the basis of the calculations and the experimental data are given in tab. 3 and drawn under the XPS as vertical bars, fig. 6(b). These data prove the RDV method to be effective and allow the quantitative MO scheme for understanding the nature of interatomic bonding in AmO_2.

The outer valence band intensity is formed mostly from the outer valence Am 5f,6d,7s,7p, and O 2p AO, and to a lesser extent from the inner valence Am 6p and O 2s AO. The Am 5f electrons contribute significantly to the OVMO intensity (tabs. 2, 3). Because the Am 5f photoemission cross-section is high (tab. 2), the Am 5f electrons contribute significantly to the OVMO XPS intensity if they do not lose the f-nature. Thus, the Am 5f electrons can be promoted to *e. g.* the Am 6d level first, and then to participate in the chemical bond formation. They also can participate directly in the formation of the interatomic bond without losing the f-nature. The electronic structure calculations for AmO_2 showed that the Am 5f electrons participate directly in the chemical bond formation (tab. 2). In the ionic approximation for americium electronic configuration Am $6s^26p^65f^76d^07s^2$ in AmO_2 the calculated OVMO/IVMO intensity ratio was found to be 3.05 [40, 74], which is slightly higher than the corresponding theoretical value 2.77 and less than the experimental value 3.3 (see tab. 3). This difference can be partially explained by the measurement error of 10 %. This intensity ratio is an important quantitative characteristic of the AmO_2 electronic structure. These results yield a conclusion that the Am 5f electrons can participate directly in the chemical bond formation in AmO_2 and they can partially lose the f-nature. These electronic states are located closer to the middle and the top of the outer valence band (tab. 2); the Am 6d electronic states are located mostly at the bottom of the

Table 3. Valence XPS parameters for AmO_2 and AmO_8 cluster (RDV), MO orbital forces f_i and the Am 6p and Am 5f electronic state densities ρ_i (e^-)

MO		$-E$ [a], [eV]	f_i, 10^{-8} N [b]	XPS Energy [c] [eV]		XPS Intensity [%]	Am 6p, 5f electronic state densities ρ_i, e^- (electrons)			
				Experiment	Theory	Experiment	$5f_{5/2}$	$5f_{7/2}$	$6p_{1/2}$	$6p_{3/2}$
OVMO	$21\gamma_7^-$ [d]	2.17	–0.05	2.2(1.8)	9.4	43.8	0.72	0.13		
	$24\gamma_6^-$	2.30	–0.11		18.5		1.78	0.04		
	$20\gamma_7^-$	2.31	–0.11		18.3		1.78	0.02		0.02
	$23\gamma_6^-$	4.12	–0.02		0.1					
	$19\gamma_7^-$	4.12	–0.02		0.1		0.10	0.04		
	$22\gamma_6^+$	4.33	–0.01		0.1		0.10	0.04		
	$19\gamma_7^+$	4.34	–0.01	4.0(1.8)	0.1	16.0				
	$21\gamma_6^+$	4.35	–0.01		0.1					
	$22\gamma_6^-$	4.54	–0.03		4.0		0.26	0.06		0.08
	$18\gamma_7^-$	4.54	–0.03		3.5		0.26	0.06		0.08
	$18\gamma_7^+$	4.60	0.01		0.1					
	$17\gamma_7^+$	4.63	0.01		0.1					
	$20\gamma_6^+$	4.64	0.01		0.1					
	$21\gamma_6^-$	4.92	0.02		2.2			0.02		
	$17\gamma_7^-$	5.23	0.02		5.6		0.28	0.22		
	$16\gamma_7^-$	5.29	0.03		1.1		0.06	0.02		0.02
	$20\gamma_6^-$	5.29	0.02		1.0		0.06	0.02		
	$19\gamma_6^-$	5.60	0.01		0.1					
	$16\gamma_7^+$	6.03	0.04	5.8(1.9)	0.4	7.7				
	$19\gamma_6^+$	6.07	0.04		0.4					
	$15\gamma_7^+$	6.06	0.04		0.4					
	$18\gamma_6^+$	6.14	0.02		0.1					
	$15\gamma_7^+$	6.66	0.05		2.3		0.10	0.10		
	$18\gamma_6^-$	6.16	0.05		2.1		0.08	0.10		
	$14\gamma_7^-$	6.18	0.05		2.3		0.14	0.06		
	$14\gamma_7^+$	6.81	0.07		0.5					
	$17\gamma_6^+$	6.82	0.07		0.5					
	Sat			8.8(3.3)		9.4				
	Σf_i [e]		0.16 [80 %]		73.5	76.9	5.12	1.03		0.20
IVMO	$17\gamma_6^-$	17.00	–0.11	17.3(2.7)	4.2	9.2				1.16
	$13\gamma_7^-$	17.00	–0.11		4.2					1.18
	$12\gamma_7^-$	19.10	0.01		1.6		0.02	0.02		
	$16\gamma_6^-$	19.51	0.01	19.4(2.4)	1.2	2.4			0.04	
	$13\gamma_7^+$	19.52	0.03		1.3					
	$12\gamma_7^+$	19.52	0.03	21.7(3.2)	1.3	5.8				
	$16\gamma_6^+$	19.52	0.03		1.3					
	$15\gamma_6^+$	20.10	0.05		1.1					
	$15\gamma_6^-$	20.99	0.08	24.1(3.0)	3.1	2.8				0.72
	$11\gamma_7^-$	20.99	0.08		3.0					0.72
	$14\gamma_6^-$	29.77	–0.06	30.8(1.9)	4.2	2.9			1.96	
	Σf_i [e]		0.04 [20 %]		26.5	23.1	0.02	0.02	2.00	3.78
	$14\gamma_6^+$	49.70		~49.8(6.0)	~5.4					

[a] Energies shifted toward the highest values (downward) by 2.17 eV; [b] orbital forces f_i (10^{-8} N) calculated for the Am bound with one ligand (O); [c] FWHM, eV given in parentheses; [d] highest occupied MO (1 electron), occupation number for the other MO is 2; [e] total values of orbital forces f_i, peak intensities and the Am 6p, 5f DOS

outer valence band. This agrees with the theoretical and the experimental data for ThO_2 [45], UO_2 [46], NpO_2 [43], and PuO_2 [42].

The peak at 8.8 eV in the OVMO XPS of AmO_2 (fig. 6) according to [19] was attributed to the multiplet splitting of the Am $5f^5$ Am(IV) spectrum. However, the similar peaks were observed in the XPS from NpO_2 [43] and PuO_2 [42], whose calculated multiplet splitting related structures for Np(IV) and Pu(IV) differ significantly from that or Am(IV) [19].

Taking into account the quasi-atomic nature of the Am $5f^5$ electrons in AmO_2, one can expect shake-up satellites at E_{sat} 6.9 eV similar to those in *e. g.* the Am 4f XPS (fig. 2). Indeed, the considered peak was observed on the higher BE side 6.6 eV away from the Am 5f peak at E_b(Am 5f) = 2.2, which agrees

approximately with E_{sat}(Am 4f) = 6.9 eV. The intensity of this satellite regarding to the Am 5f peak intensity is I_{sat} = 18 % (tab. 2). This value agrees with the fact that the shake-up satellite intensity decreases as the BE decreases [39, 42].

In the IVMO XPS BE range a satisfactory agreement was reached *e. g.* for the $17\gamma_6^-$, $13\gamma_7^-$ (5), and $14\gamma_6^-$ (9) MO responsible for the width E of this XPS band. The calculated E_{Theor} = 12.77 eV agrees with the experimental E_{exp} = 13.5 eV (tab. 2). It has to be noted that the theoretical (2.73) and experimental (3.3) OVMO/IVMO intensity ratios are comparable; that confirms correctness of the approximations used in the calculation (tab. 2). The calculated and the experimental relative intensities of some individual IVMO peaks, except for the $17\gamma_6^-$, $13\gamma_7^-$ (5) ones, are in a qualitative agreement. The worst discrepancy was observed for the $15\gamma_6^-$, $11\gamma_7^-$ (8), and $14\gamma_6^-$ IVMO.

Taking into account the experimental BE differences between the outer MO and the core levels in AmO_2 and atomic Am [59], as well as the relativistic calculation data for the AmO_8 cluster in the MO LCAO approximation, a quantitative MO scheme for AmO_2 (fig. 8), was built. This scheme enables one to under-

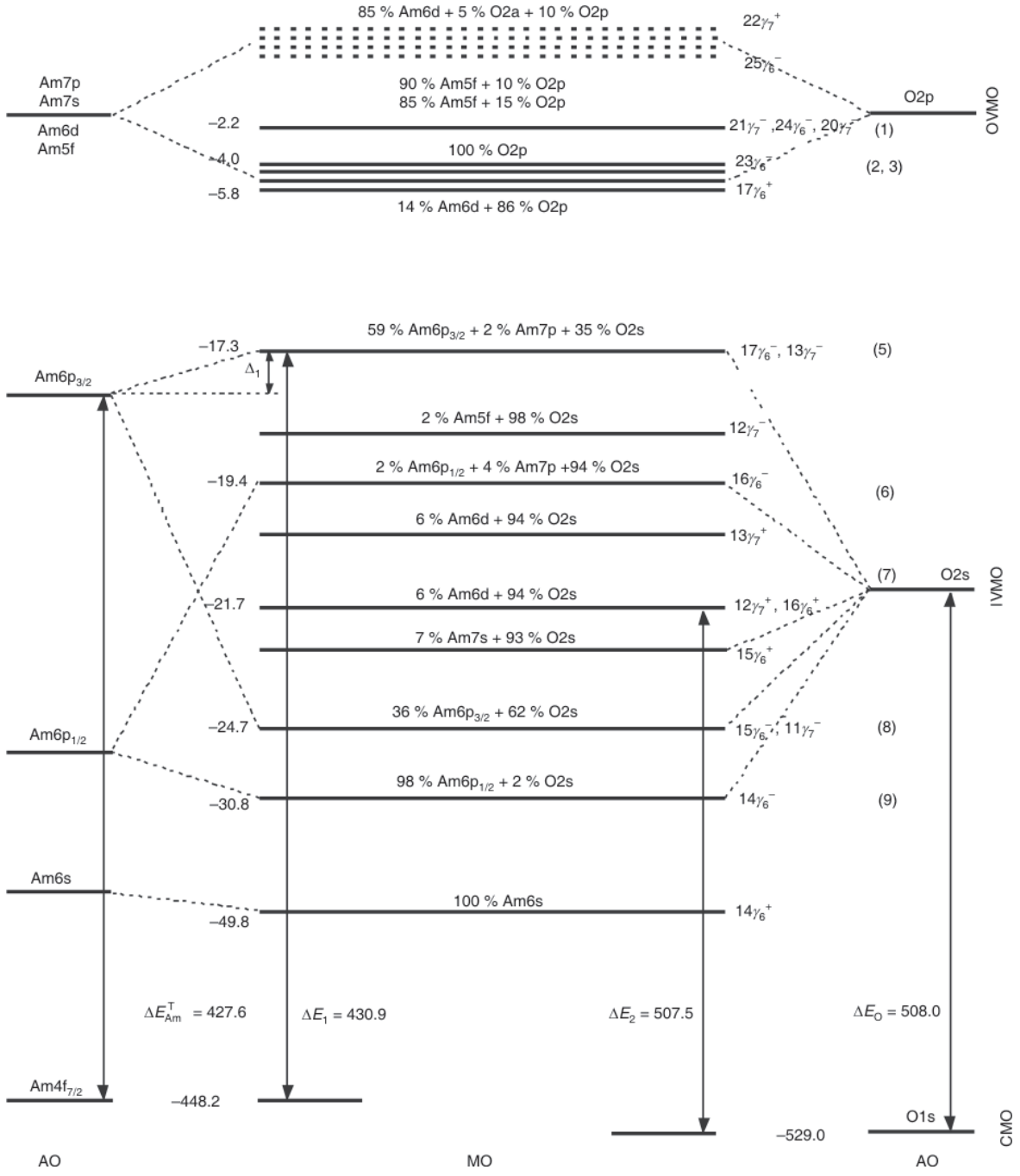

Figure 8. MO scheme for the AmO_8 cluster built taking into account theoretical and experimental data. Chemical shifts are not indicated. Arrows show the measured differences in BE between selected levels. Experimental BE [eV] are given to the left. The energy scale is omitted

stand the real XPS structure and the chemical bond nature in AmO_2. In this approximation, one can pick out the antibonding $17\gamma_6^-$, $13\gamma_7^-$ (5), and $16\gamma_6^-$ (6) and the corresponding bonding $15\gamma_6^-$, $11\gamma_7$ (8), and $14\gamma_6^-$ (9) IVMO, as well as the quasi-atomic $12\gamma_7^-$, $13\gamma_7^+$, $12\gamma_7^+$, $16\gamma_6^+$, and $15\gamma_6^+$ (7) ones attributed mostly to the O 2s electrons. The experimental data show that the O 2s-related quasi-atomic IVMO BE have to be close by magnitude. Indeed, the O 1s XPS of AmO_2 allows a suggestion that their chemical non-equivalence should not exceed ~1 eV, since the O 1s peak was observed symmetric and 1.3 eV wide. The O 2s BE has to be about 21 eV, since the E_O = 508 eV and the O 1s BE in AmO_2 is E_b = 529.0 eV (fig. 1). The theoretical results agree partially with these data. Taking into account that the calculated BE difference between E_b(Am $4f_{7/2}$) = = 450.84 eV and E_b(Am $6p_{3/2}$) = = 23.29 eV is E^T_{Am}= = 427.6 eV [59], which agrees with the corresponding experimental BE difference between the Am $6p_{3/2}$ peak at 18.4 eV and the low BE line at 446.4 eV in the Am $4f_{7/2}$ spectrum of metallic Am being 428.0 eV [7], E_1 = 430.9 eV, one can find that $_1$ = 3.3 eV (fig. 8). It confirms the antibonding nature of the $17\gamma_6^-$, $13\gamma_7^-$ (5) IVMO. Since the BE difference between the $17\gamma_6^-$, $13\gamma_7^-$ (5), and $14\gamma_6^-$ (9) IVMO is 13.5 eV, and the Am 6p spin-orbit splitting according to the calculation data of [59] is E^T_{sl}(Am 6p) = 12.55 eV, one can see that the perturbation $_1$ ~1.0 eV does not agree with the corresponding value of 3.3 eV found from the BE difference between the core and the valence MO. This difference must be attributed to the IVMO formation and such a comparison is probably not quite correct. The IVMO FWHM cannot yield a conclusion on the IVMO nature (bonding or antibonding), however, one can suggest that the admixture of 4 % of the O 2p and 2 % of the Am 7p AO in the $17\gamma_6^-$, $13\gamma_7^-$ (5) IVMO leads these orbitals to loosing of their antibonding nature (tab. 2, fig. 8, see also [38]). Thus, the quantitative MO scheme for AmO_2 built on the basis of the experimental and the theoretical data allows one both to understand the nature of chemical bond formation in AmO_2 and to interpret the structures of other X-ray spectra of AmO_2 as it was shown for ThO_2 [45], UO_2 [46], NpO_2 [43], and PuO_2 [42].

O KLL Auger spectrum structure of AmO_2

The MO scheme for AmO_2 (fig. 8) was used to explain qualitatively the Auger O KLL spectral structure of AmO_2. For example, the O KLL Auger spectrum of Al_2O_3 is known to consist of three strong but unstructured ~9 eV wide peaks reflecting the O $KL_{2-3}L_{2-3}$ (O 1s O2p), the O KL_1L_{2-3} (O1s O2s, 2p) and the O KL_1L_1 (O1s O2s) transitions [75]. The relative intensities of these Auger O KLL peaks are given as the Auger O KLL to the O 1s XPS intensity ratios. These relative intensities are important fundamental values. They allow a quantitative comparison of, for example, the O 2p partial DOS on oxygen ions in various oxides [75].

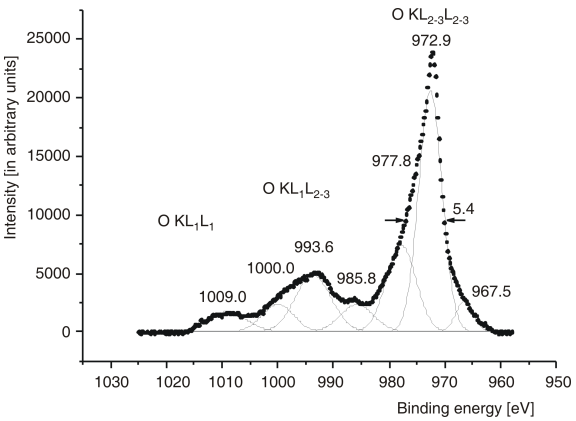

Figure 9. Auger O KLL spectrum from AmO_2

The Auger spectrum of AmO_2 consists of three bands (fig. 9). Unfortunately, at the higher BE side these bands exhibit shoulders due to the impurity oxygen on the sample surface. Despite this, a qualitative interpretation of this spectrum is possible. For example, the Auger O $KL_{2-3}L_{2-3}$ (O1s O2p) (Γ = 5.4 eV) spectrum at 972.9 eV BE of AmO_2 reflects the filled O 2p DOS in AmO_2 (fig. 9). The O $KL_{2-3}L_{2-3}$ FWHM is comparable with the FWHM sum of the XPS O 1s electron peak (Γ =1.3 eV, fig. 1) and the O 2p DOS (peaks 2 and 3) in AmO_2 (Γ~3.7 eV, fig. 8, tab. 3). The O KL_1L_{2-3} (O 1s O 2s, 2p) peak reflects both the O 2p, and the O 2s DOS. This peak is complicated (consists of three lines) and hardly interpretable. The O KL_1L_1 (O 1s O 2s) peak reflecting mostly the DOS of the O 2s electrons participating in the formation in AmO_2 is highly structured. The FWHM of this peak Γ ~13 eV is comparable to that of the IVMO in the XPS spectrum. It confirms the participation of the O 2s electrons in the IVMO formation (figs. 6, 8). These results agree with the O KLL Auger data for ThO_2 [45] UO_2 [46] NpO_2 [43], and PuO_2 [42].

Chemical bond in the AmO_8 cluster

As it was noted, the calculation data show that the MO system of the AmO_8 cluster can be subdivided into three groups (tab. 2, fig. 8). The first one represents the outer valence band, OVMO: $21\gamma_7^-$ to $17\gamma_6^+$ (1-3), with the bonding MO and the admixture of the valence Am 6d states in the lower part. The second one consists of the IVMO formed mostly from the Am 6p and the O 2s AO of the neighboring americium and oxygen $17\gamma_6^-$, $13\gamma_7^-$ (5), $16\gamma_6^-$ (6), $15\gamma_6^-$, $11\gamma_7^-$ (8), $14\gamma_6^-$ (9). The third one represents the quasi-atomic IVMO ($12\gamma_7^-$, $13\gamma_7^+$, $12\gamma_7^+$, $16\gamma_6^+$, $15\gamma_6^+$ (7), $14\gamma_6^+$) with small admixtures of the outer americium AO (tab. 2).

At the present time there is no method to evaluate quantitative contribution of certain separate MO into the chemical bond even for diatomic molecules [38]. Such a method has to be additive, *i. e*., the summation of contributions of separate MO with electron populations in mind, has to yield the total chemical bond value. The work [38] considers three methods of evaluation of the MO nature (bonding, non-bonding, antibonding) on the basis of: (a) population by Mulliken, (b) full energy separation with subtraction of resonance energy characterizing the covalence of the chemical bond, and (c) orbital forces.

In the Koopmans' theorem approximation, the orbital forces f_i (10^{-8} N) approximately are equal to the derivatives of the MO energies E_i' (10^{-8} N) upon the interatomic distances [38]. Therefore, this work presents the dependence of the MO energies for the AmO_8 (D_{4h}) cluster on the interatomic distance $R_{Am\text{-}O}$. To evaluate the orbital forces in addition to the calculation for the equilibrium atomic positions ($R_{Am\text{-}O}$ = 0.2329 nm), a calculation for $R_{Am\text{-}O}$ = 0.2349 nm was also done. It yielded the orbital forces f_i (derivatives E_i' of the OVMO and IVMO energies E_i upon the interatomic distances $R_{Am\text{-}O}$ for the AmO_8 cluster) (tab. 3).

The structures of irreducible representations of the D_{4h} group allows comparisons of the Pu 6d and the Pu 5f AO participation in the chemical bond since the γ_6^+ and the γ_7^+ contain the 6d states and do not contain the 5f states, while the γ_6^- and the γ_7^- – *vice versa*, contain the 5f states and do not contain the 6d states. The fraction of the 6d AO in the bonding OVMO from $17\gamma_6^+$ to $21\gamma_6^-$ in the lower MO part is 0.57, while the fraction of the 5f AO – 0.72 (tab. 2). Despite the fact that the fraction of the 5f AO is greater than the corresponding fraction of the 6d AO, their contributions are comparable. Thus, the $14\gamma_6^+$ and the $17\gamma_6^+$ MO exhibit the highest orbital force (0.07 10^{-8} N) among the considered bonding OVMO. So, the binding role of the 6d states in the Am – O interaction is slightly higher than that of the 5f states.

As it was expected, the binding OVMO of the lower valence band part (from the $17\gamma_6^+$ to the $18\gamma_7^+$) contribute significantly (0.56 10^{-8} N) in the Am-O binding despite the anti-bonding nature of the other OVMO (–0.40 10^{-8} N). It has to be noted that the so-called "quasi-atomic" Am5f electrons ($4.47e^-$) in reality are localized on the anti-bonding $21\gamma_6^-$, $21\gamma_6^-$, $17\gamma_6$+ IVMO and weaken significantly the binding (–0.27 10^{-8} N). It is about 40 % of all the anti-bonding nature of the valence electrons. The total contribution of the OVMO electrons in the Am – O binding per one ligand is 0.16 10^{-8} N (tab. 2).

The $17\gamma_6^-$ and $13\gamma_7$ IVMO electrons bring a significant anti-bonding contribution (–0.22 10^{-8} N) in the Am – O binding, and the $15\gamma_6^-$ and $11\gamma_7^-$ IVMO electrons bring some lower bonding contribution into (0.16 10^{-8} N) in the binding per a ligand (tab. 3, fig. 8). As a result, electrons of these anti-bonding ($17\gamma_6^-$, $13\gamma_7^-$) and corresponding bonding ($15\gamma_6^-$, $11\gamma_7$) IVMO weaken the Am-O bond. On the other hand, electrons of the quasi-atomic $12\gamma_7^-$–$15\gamma_6^+$ IVMO contributed from the outer valence AO bring a significant bonding contribution (0.16 10^{-8} N) in the Am-O interaction.

The MO scheme (fig. 8) shows that formally the $14\gamma_6^-$ IVMO is supposed to be slightly bonding. However, the calculation shows that this MO is anti-bonding (–0.06 10^{-8} N). Since the $14\gamma_6^-$ IVMO contains 98 % of the Am $6p_{1/2}$ and only 2 % of the O 2s AO, by its nature it is close to the atomic Am $6p_{1/2}$ AO, which can be to a lesser extent screened from the effective nuclear changing as the interatomic distance grows. This results in a significant increase of the $14\gamma_6^-$ IVMO energy due to the chemical shift, which does not depend on the direct participation of the Am $6p_{1/2}$ in the chemical bond (tab. 3). Since the Am 6s AO practically does not participate in the IVMO formation (tab. 2), it was not taken into account. As a result it was found that the IVMO electrons calculated for the binding with one ligand Am-O strengthen the chemical bond (0.04 10^{-8} N).

The evaluation per one ligand of the Am-O binding yielded that the total contribution of the OVMO and IVMO electrons is 0.20 10^{-8} N, the OVMO relative contribution is 80 %, and the IVMO relative contribution is 20 %. The obtained orbital forces f_i are in a good agreement with the calculation results for the diatomic molecules of the second period of the periodic table taking into account a significant difference in the interatomic distances $R_{Am\text{-}O}$ = 0.2329 and *e. g*., $R_{O\text{-}O}$ = 0.1207 for O_2 [38]. Although the obtained data are approximate, they allow a conclusion that the IVMO formation should not be neglected when studying the chemical bond nature in actinide compounds.

CONCLUSIONS

The XPS structure of AmO_2 was studied in the binding energy range 0 eV-1250 eV. The correlation of the XPS structure parameters with the mechanisms of its formation were established. With the BE differences between the core and valence electronic levels and the relativistic calculation results of the electronic structure of the AmO_8 cluster in mind, a quantitative interpretation of the XPS structure of the OVMO (0 eV to ~15 eV BE) and the IVMO (~15 eV to ~35 eV BE) for americium dioxide AmO_2 was done. The Am 5f (1.72 Am 5f e^-) electrons delocalized within the outer valence band were theoretically shown and experimentally confirmed to participate directly in the chemical bond formation in AmO_2, partially losing their *f*-nature. The other part of the Am 5f electrons (4.47 Am 5f e^-) was shown to be localized mostly at 2.2 eV. The Am 6p electrons, in addition to the effective (experimentally measurable) participation in the IVMO formation, were found to contribute noticeably (~0.2

Am 6p e^-) in the occupied part of the OVMO in AmO_2. The results of our investigation showed that the largest role in the IVMO formation in AmO_2 was played by the Am $6p_{3/2}$ and the O 2s AO of the neighboring neptunium and oxygen ions. On moving from ThO_2 to UO_2, NpO_2, PuO_2, and AmO_2 one can observe the An 5f DOS growth in the valence band and the An 5f BE growth starting with UO_2. A small (~1 eV) change in the An $6p_{3/2}$ BE confirms the valence nature of the An $6p_{3/2}$ electrons. The An $6p_{3/2}$ – O 2s interaction in this row is significant. The increase of the spin-orbit interaction in the considered row causes the An $6p_{1/2}$ BE change of ~5.9 eV. It weakens significantly the An $6p_{1/2}$ – O 2s-interaction. Contributions of different MO electrons to the chemical bond in the AmO_8 cluster were evaluated. The MO sequent order in the BE range of 0-~35 eV for AmO_2 was defined and the corresponding MO composition was obtained in the cluster calculations. This yielded a fundamental quantitative MO scheme, which is important for understanding the nature of interatomic bonding in AmO_2 and for the interpretation of other X-ray spectra of AmO_2. The general laws of the valence electronic structure changes on moving from ThO_2 to UO_2, NpO_2, PuO_2, and AmO_2 were found.

ACKNOWLEDGEMENT

This work was supported by the RFBR grant #13-03-00214-a and partially supported by M. V. Lomonosov Moscow State University Program of Development.

AUTHOR CONTRIBUTIONS

The idea for the study was put forward by Yu. A. Teterin, the measurements were carried out by K. I. Maslakov, and the theoretical calculations were carried out by M. V. Ryzhkov. The samples were prepared, the experimental data were processed and interpreted by A. Yu. Teterin, K. E. Ivanov, S. N. Kalmykov and V. G. Petrov.

REFERENCES

[1] Walter, M., *et al*., Local Atomic Structure of a Zirconia-Based Americium Transmutation Fuel, *J. Solid State Chemistry, 180* (2007), 11, pp. 3130-3135

[2] Naegele, J. R., Ghijsen, J., Manes, L., Localization and Hybridization of 5f States in the Metallic and ionic Bond as Investigated by Photoelectron Spectroscopy, *Struct. Bonding, 59-60* (1985), *Chapter E,* pp. 197-262

[3] Moore, K. T., Van der Laan, G., Nature of the 5f States in Actinide Metals, *Rev. Mod. Phys., 81* (2009), 1, pp. 235-298

[4] Naegele, J. R., *et al*., Localisation of 5f Electrons in Americium: Photoemission Study, *Phys. Rev. Lett., 52* (1984), 20, pp. 1834-1837

[5] Martenson, N., Johansson, B., Naegele, J. R., Possible Interpretation of the Photoelectron Spectrum for Americium Metal, *Phys. Rev. B, 35* (1987), 3, pp. 1437-1439

[6] Naegele, J. R., Surface Analysis of Actinide Materials, *J. Nucl. Mater., 166* (1989), 2, pp. 59-67

[7] Cox, L. E., Ward, J. W., Haire, R. G., X-Ray Photoemission Spectroscopy Study of the Electronic Structure of Am Metal and AmH_x (for x 2), *Phys. Rev., B 45* (1992), 23, pp. 13239-13243

[8] Gouder, T., *et al*., Photoemission Study of the Electronic Structure of Am, AmN, AmSb, and Am_2O_3 films, *Phys. Rev., B, 72* (2005), pp. 115-122

[9] Shick, A., *et al*., Electronic Structure and Nonmagnetic Character of δ-Pu-Am Alloys, *Phys. Rev. B, 73* (2006), 104415

[10] Moore, K. T., *et al*., Rampant Changes in $5f_{5/2}$ and $5f_{7/2}$ Filling Across the Light and Middle Actinide Metals: Electron Energy-Loss Spectroscopy, Many-Electron Atomic Spectral Calculations, and Spin-Orbit Sum Rule, *Phys. Rev., B, 76* (2007), 073105

[11] Baclet, N., *et al*., Character of 5f States in the Pu-Am System from Magnetic Susceptibility, Electrical Resistivity, and Photoelectron Spectroscopy Measurement, *Phys. Rev., B, 75* (2007), 035101

[12] Butterfield, M. T., *et al*., Understanding the $O_{4,5}$ Edge Structure of Actinide Metals: Electron Energy-Loss Spectroscopy and Atomic Spectral Calculations of Th, U, Np, Am, and Cm, *Phys Rev. B, 77* (2008), 1, 13109

[13] Skriver, H. L., Andersen, O. K., Johansson, B., Calculated Bulk Properties of the Actinide Metals, *Phys. Rev. Lett., 41* (1978), 1, pp. 42-45

[14] Skriver, H. L., Andersen, O. K., Johansson, B., 5*f*-Electron Delocalization in Americium, *Phys. Rev. Lett., 44* (1980), 18, pp. 1230-1233

[15] Johansson, B., Energy Position of the 5f Level in Americium Metal, *Phys. Rev. B., 30* (1984), 6, pp. 3533-3535

[16] Soderlind, P., Landa, A., Crystal Stability and Equation of State for Am: Theory, *Phys. Rev. B, 72* (2005), 2, 024109

[17] Savrasov, S. Y., Haule, K. H., Kotliar, G., Many-Body Electronic Structure of Americium Metal, *Phys. Rev. Lett., 96* (2006), p. 036404

[18] Mayer, K., *et al*., On the Valency State of Americium in $(U_{0.5}Am_{0.5})O_{2-x}$, *J. Alloys Compd., 213-214* (1994), pp. 456-459

[19] Veal, B. W., Diamond, H., Hoekstra, H. R., X-Ray Photoelectron-Spectroscopy Study of Oxides of the Transuranium Elements Np, Pu, Am, Cm, Bk, and Cf, *Phys. Rev., B 15* (1977), 6, pp. 2929-2942

[20] Nishi, T., *et al*., EXAFS and XANES Studies of Americium Dioxide with Fluorite Structure, *J. Nucl. Mater., 374* (2008), 3, pp. 339-343

[21] Martin, P. M., *et al*., EXAFS Study of the Structural Phase Transition in the Americium Zirconate Pyrochlore, *J. Nucl. Mater., 385* (2009), 1, pp. 126-130

[22] Seibert, A., Gouder, T., Huber, F., Formation and Stability of Actinide Oxides: A Valence Band Photoemission Study, *Radiochemica Acta, 97* (2009), 4-5, pp. 247-250

[23] Nishi, T., et al., Local and Electronic Structure of Am_2O_3 and AmO_2 with XAFS Spectroscopy, *J. Nucl. Mater., 401* (2010), 1-3, pp. 138-142

[24] Prieur, D., *et al*., Local Structure and Charge Distribution in Mixed Uranium–Americium Oxides: Effects of Oxygen Potential and Am content, *Inorg. Chem., 50* (2011), 24, pp. 12437-12445

[25] Vespa, M., *et al*., Fabrication and Characterization of $(U, Am)O_{2-x}$ transmutation Targets, *J. Nucl. Mater., 421* (2012), 1-3, pp. 80-88

[26] Gubanov, V. A., Rosen, A., Ellis, D. E., Electronic Structure and Chemical Bonding in Actinide Oxides:

Monoxides and Dioxides of Np, Pu, Am,Cm, and Bk, *Journal of Physics and Chemistry of Solids, 40* (1979), 1, pp. 17-28
[27] Prodan, I. D., Scuseria, G. E., Martin, R. L., Covalency in the Actinide Dioxides: Systematic Study of the Electronic Properties Using Screened Hybrid Density Functional Theory, *Phys. Rev., B 76* (2007), 033101
[28] Suzuki, C., *et al*., Calculation of the Electronic Structure of AmO_2 and Pr_6O_{11} for XANES Analysis with Redox Property, *J. Quantum Chem., 109* (2009), 12, pp. 2744-2752
[29] Petit, L., *et al.*, Electronic Structure and Ionicity of Actinide Oxides from First Principles, *Phys. Rev., B 81* (2010), 045108
[30] Wen, X.-D., *et al*., Effect of Spin-Orbit Coupling on the Actinide Dioxides AnO_2 (An = Th, Pa, U, Np, Pu, and Am): A Screened Hybrid Density Functional Study, *J. Chem. Phys., 137* (2012), 154707
[31] Suzuki, C., *et al*., Core-Hole Effect on XANES and Electronic Structure of Minor Actinide Dioxides with Fluorite Structure, *Journal of Physics and Chemistry of Solids, 73* (2012), 2, pp. 209-216
[32] Wen, X.-D., *et al*., Density Functional Theory Studies of the Electronic Structure of Solid State Actinide Oxides, *Chem. Rev., 113* (2013), 2, pp. 1063-1096
[33] Suzuki, C., *et al*., DFT Study on the Electronic Structure and Chemical State of Americium in an (Am, U) Mixed Oxide, *Journal of Physics and Chemistry of Solids, 74* (2013), 12, pp. 1769-1774
[34] Lu, Y., *et al*., Electronic, Mechanical, and Thermodynamic Properties of Americium Dioxide, *J. Nucl. Mater., 441* (2013), 1-3, pp. 411-420
[35] Nishi, T., *et al*., Valence State of Am in $(U_{0.95}Am_{0.05})O_{2.0}$, *J. Nucl. Mater., 418* (2011), 1-3, pp. 311-312
[36] Teterin, Yu. A., *et al*., X-Ray Photoelectron Study of Actinide (Th, U, Pu, Am) Nitrates, *Nucl Technol Radiat, 18* (2003), 2, pp. 31-35
[37] Moore, K. T., *et al*., Rampant Changes in $5f_{5/2}$ and $5f_{7/2}$ Filling a Cross the Light and Middle Actinide Metals: Electron Energy-Loss Spectroscopy, Many-Electron Atomic Spectral Calculations, and Spin-Orbit Sum Rule, *Phys. Rev. B, 76* (2007), 073105
[38] Teterin, Yu. A., Gagarin, S. G., Inner Valence Molecular Orbitals and Structure of X-ray Photoelectron Spectra, *Russian Chemical Reviews, 65* (1996), 10, pp. 825-847
[39] Teterin, Yu. A., Teterin, A. Yu., Structure of X-Ray Photoelectron Spectra of Lanthanide Compounds, *Russian Chemical Reviews, 71* (2002), 5, pp. 347-381
[40] Teterin, Yu. A., Teterin, A. Yu., Structure of X-Ray Photoelectron Spectra of Light Actinide Compounds, *Russian Chemical Reviews, 73* (2004), 6, pp. 541-580
[41] Teterin, Yu. A., *et al*, Electronic Structure and Chemical Bonding in PuO_2, *Phys. Rev. B, 87* (2013), 245108
[42] Teterin, A. Yu., *et al*., Electronic Structure of Solid Uranium Tetrafluoride UF_4, *Phys. Rev. B, 74* (2006), 045101
[43] Teterin, Yu. A., *et al*., X-Ray Photoelectron Spectroscopy Structure and Chemical Bond Nature in NpO_2, *Phys. Rev. B, 89* (2014), 035102
[44] Teterin, Yu. A., *et al*., A Study of Synthetic and Natural Uranium Oxides by X-Ray Photoelectron Spectroscopy A Study of Synthetic and Natural Uranium Oxides by X-Ray Photoelectron Spectroscopy, *Physics and Chemistry of Minerals, 7* (1981), 4, pp. 151-158
[45] Teterin, A. Y., *et al*., Emission of ThO_2 Valence Electrons upon Excitation with Synchrotron Radiation Near the $O_{4,5}$(Th) Resonance Absorption Threshold, *Radiochemistry, 51* (2009), 6, pp. 560-566
[46] Teterin, Yu. A., Teterin, A. Yu., X-Ray Spectral Methods in Investigation of the UO_2 Electronic Structure, *Radiochemistry, 47* (2005), pp. 440-446
[47] Teterin, A. Yu., *et al*., Nature of Chemical Bonding in ThF_4, *Radiochemistry, 51* (2009), 6, pp. 551-559
[48] Teterin, Yu. A., Baev, A. S., X-Ray Photoelectron Spectroscopy of Light Actinide Compounds (in Russian), Moscow, TsBIIatominform, 1986, p. 104
[49] Utkin, I. O., *et al*., X-ray Spectral Studies of the Electronic Structure of Uranyl Fluorite UO_2F_2, *Nucl Technol Radiat, 19* (2004), 2, pp. 15-23
[50] Teterin, A. Yu., et al., X-Ray Spectroscopic Study of U 6p, 5f Electronic Levels in γ-UO_3, *Radiochemistry, 44* (2002), 3, pp. 224-233
[51] Shirley, D. A., High-Resolution X-Ray Photoemission Spectrum of the valence Bands of Gold, *Phys. Rev., B 5* (1972), 15, pp. 4709-4713
[52] Gouder T., Havela, L., Mikrochim, Examples of Quantification in XPS on 5f Materials, *Radiochemica Acta, 138* (2002), 3-4, pp. 207-215
[53] Chikalla, T. D., Eyring, L., Phase Relations in the Americium Oxygen System, *Journal of Inorganic and Nuclear Chemistry, 30* (1968), 1, pp. 133-145
[54] Rosen, A., Ellis, D. E., Relativistic Molecular Calculations in the Dirac-Slater Model, *J. Chem. Phys., 62* (1975), 8, pp. 3039-3049
[55] Adachi, H., Relativistic Molecular Orbital Theory in the Dirac-Slater Model, *Technol. Reports Osaka Univ., 27* (1977), 1392, pp. 569-576
[56] Gunnarsson, O., Lundqvist, B. I., Exchange and Correlation in Atoms, Molecules and Solids by the Spin-Density-Functional Formalism, *Phys. Rev. B, 13* (1976), pp. 4274-4298
[57] Pyykko, P., Toivonen, H., Tables of Representation and Rotation Matrices for the Relativistic Irreducible Representations of 38 Point Groups, *Acta Acad. Aboensis, Ser. B, 43* (1983), 2, pp. 1-50
[58] Varshalovish, D. A., Moskalev, A. N., Khersonskii, V. K., Quantum Theory of Angular Momentum, World Scientific, Singapore, 1988
[59] Huang, K. N., *et al*., Neutral-Atom Electron Binding Energy from Relaxed-Orbital Relativistic Hartree-Fock-Slater Calculations, *At. Data Nucl. Data Tables, 18* (1976), 3, pp. 243-291
[60] Van Vleck, J. H., The Dirac Vector Model in Complex Spectra, *Phys. Rev., 45* (1934), pp. 405-409
[61] Sham, T. K., Wendin, G., Screening and Configuration-Interaction Effects in the 5p X-Ray-Photoelectron Spectrum of Th Metal, *Phys. Rev. Lett., 44* (1980), 12, pp. 817-820
[62] Bancroft, G. T., Sham, T. K., Larsson, S., Configuration Interaction Satellites in the ESCA Spectra of Thorium and Other Actinide Compounds, *Chem. Phys. Lett., 46* (1977), 3, pp. 551-557
[63] Boring, M., Cowan, R. D., Martin, R. L., Satellite Structure in the 5p and 5s X-Ray Photoelectron Spectra of the Actinides, *Phys. Rev. B, 23* (1981), 2, pp. 445-448
[64] Yarzhemsky, V. G., Teterin, Y. A., Sosulnikov, M. I., Dynamic Dipolar Relaxation in X-Ray Photoelectron Spectra of Ba4p Subshell in Barium Compounds, *J. Electron Spectrosc. Relat. Phenom., 59* (1992), 3, pp. 211-222
[65] Yarzhemsky, V. G., *et al*., XPS Structure Xe and Cs, Ba, La Compounds (in Russian), *J. of Surface Investigations: X-ray, Synchrotron and Neutron Techniques, 6* (2005), pp. 3-8
[66] Amusia, M., Chernysheva, L., Yarzhemsky, V., Handbook of Theoretical Atomic Physics: Data for Photon

Absorption, Electron Scattering, and Vacancies Decay. Springer, 2012
[67] Sevier, K. D., Atomic Electron Binding Energy, *At. Data Nucl. Data Tables, 24* (1979), 4, pp. 323-371
[68] Tobin, J. G., *et al*., Resonant Photoemission in f-Electron Systems: *Pu and Gd, Phys. Rev., B 68* (2003), 155109
[69] Teterin, A. Yu., *et al*., Valence Electronic State Density in Thorium Dioxide, *Nucl Technol Radiat, 23* (2008), 2, pp. 34-42
[70] Teterin, Yu. A., Teterin, A. Yu., Modern X-Ray Spectral Methods in the Study of the Electronic Structure of Actinide Compounds: Uranium Oxide UO_2 as an example, *Nucl Technol Radiat, 19* (2004), 2, pp. 3-14
[71] Yarzhemsky, V. G., *et al*., Photoionization Cross-Sections of Ground and Excited Valence Levels of Actinides, *Nucl Technol Radiat, 27* (2012), 2, pp. 103-106
[72] Slater, J. C., Johnson, K. H., Self-Consistent-Field X Cluster Method for Polyatomic Molecules and Solids, *Phys. Rev., B 5* (1972), 3, pp. 844-853
[73] Band, M., Kharitonov, Yu. I., Trzhaskovskaya, M. B., Photoionization Cross-Sections and Photoelectron Angular Distributions for X-Ray Line Energies in the Range 0.132 keV-4.509 keV (Targets: 100 Z 1), *At. Data Nucl. Data Tables, 23* (1979), 5, pp. 443-505
[74] Teterin, Y. A., *et al*., XPS Study of the An5f Electronic States in Actinide (Th, U, Np, Pu, Am, Cm, Bk) Compounds, *J. Nucl. Sci. Technol. Suppl., 3* (2002), pp. 140-143
[75] Teterin, Y. A., *et al*., Auger and X-Ray Photoelectron Spectroscopy Study of the Density of Oxygen States in Bismuth, Aluminum, Silicon and Uranium Oxides, *J. Electron Spectrosc. Relat. Phenom., 101-103* (1999), 1-3, pp. 401-405

Received on May 6, 2015
Accepted on May 19, 2015

Јурий А . ТЕТЕРИН, Константин И. МАСЛАКОВ, Михаил В. РИЖКОВ, Антон Ј. ТЕТЕРИН, Кирил Е. ИВАНОВ, Степан Н. КАЛМИКОВ, Владимир Г. ПЕТРОВ

СТРУКТУРА РЕНДГЕНСКИХ ФОТОЕЛЕКТРОНСКИХ СПЕКТАРА И ХЕМИЈСКЕ ВЕЗЕ У АМЕРИЦИЈУМДИОКСИДУ

Обављена је квантитативна анализа структуре рендгенских фотоелектронских спектара у области енергија везе од 0 eV до 35 eV валентних електрона америцијумдиоксида. При томе су урачунате енергије везе и структуре електронских љуски језгра (35 eV-1250 eV), као и резултати релативистичких дискретних варијационих прорачуна $Am_{63}O_{216}$ и AmO_8 (D_{4h}) кластера који одражавају блиску околину америцијума у америцијумдиоксиду. Експериментални подаци показују да ефекти више тела и вишеструког цепања доприносе спектралној структури много мање од ефеката састава спољашњих (енергија везе 0-~15 eV) и унутрашњих (енергија везе ~15 eV-~35 eV) валентних молекулских орбитала. Показано је да се у валентној зони америцијумдиоксида формирају унета Am 5f електронска стања и да Am 5f електрони учествују у саставу и унутрашњих и спољашњих валентних молекулских орбитала (зона). Нађено је да унете Am $6p_{3/2}$ и O 2s електронске љуске дају највећи допринос образовању унутрашњих валентних молекулских орбитала. Процењени су доприноси електрона из различитих молекулских орбитала хемијској вези кластера AmO_8. У америцијумдиоксиду установљена је композиција и секвенцијални поредак молекулских орбитала у области енергија веза 0-~35 eV. Експериментални и теоријски резултати омогућавају квантитативни преглед молекулских орбитала америцијумдиоксида, што је битно и за разумевање природе хемијских веза у америцијумдиоксиду и за тумачење других спектара Х-зрачења у њему.

Кључне речи: актинид, Х-зрачење, фотоелектронски спектар, валентна молекулска орбита